Emergence of antiphase bursting in two populations of randomly spiking elements

Oleg V. Maslennikov* and Dmitry V. Kasatkin
Institute of Applied Physics of RAS, 603950, 46 Ulyanov Str., Nizhny Novgorod, Russia

Nikolai F. Rulkov
Institute for Nonlinear Science, University of California, San Diego, La Jolla, California 92093-0402, USA

Vladimir I. Nekorkin
Institute of Applied Physics of RAS, 603950, 46 Ulyanov Str., Nizhny Novgorod, Russia
and Nizhny Novgorod State University, 603950, 23 Gagarin Av., Nizhny Novgorod, Russia
(Received 17 June 2013; published 11 October 2013)

Animal locomotion activity relies on the generation and control of coordinated periodic actions in a central pattern generator (CPG). A core element of many CPGs responsible for the rhythm generation is a pair of reciprocally coupled neuron populations. Recent interest in the development of highly reduced models of CPG networks is motivated by utilization of CPG models in applications for biomimetic robotics. This paper considers the use of a reduced model in the form of a discrete time system to study the emergence of antiphase bursting activity in two reciprocally coupled populations evoked by the postinhibitory rebound effect.

DOI: 10.1103/PhysRevE.88.042907 PACS number(s): 05.45.−a, 87.18.Sn

I. INTRODUCTION

The onset of switching activity in groups of reciprocally coupled populations of neurons is a typical element of many central pattern generators (CPGs) responsible for production and control of rhythmic motor activity in animals [1–5]. A great deal of neurobiological studies of CPG circuits in experiments with animals and in theoretical studies of corresponding computational models capturing neuronal behavior at various levels of details demonstrated the important role of dynamical mechanisms involved into the generation of rhythm and its control [6–8]. A rather common network circuit found in many CPG networks is a half-center oscillator that acts as a core of rhythm generation and control [9–11]. Many half-center oscillators are formed by two neurons or two groups of neurons linked together by a reciprocal inhibition [12–14]. Such simple networks play an important role in the control of motor activity patterns such as walking, flying, and swimming.

A relatively recent development in studies of various CPG models was motivated by potential applications of neurobiological principles for the control of motor activity in biomimetic robots [15,16]. A very important element of such modeling is the design of very simple and computationally efficient models of neuronal behavior that are sophisticated enough to capture important dynamical mechanisms of real neurons and networks of neurons and can be simulated in real time within a compact low-power computer implemented with a field-programmable gate array or digital signal processor chip [17,18]. The reduction of the computational complexity here is achieved by the design of a low-dimensional model of the neuron that captures the important dynamical properties of real neurons and by scaling down the redundancy of the network in which a population of similar neurons operating together as a network node is replaced by a single-neuron model. A significant reduction of model complexity for the description of neuronal behavior can be achieved by using a map-based approach [19–24]. The reduction of the network size is a typical approach used in many simulations of big networks (see, for example, [6,17]).

In this paper we study how the network reduction affects the dynamical properties of half-center oscillations in the populations of reciprocally inhibiting neurons [see Fig. 1(a)]. We focus on the case of intrinsically not bursting neurons in which the onset of switching antiphase oscillations is supported by the effect of postinhibitory rebound (PIR) bursts. The neurons within each group do not interact with each other, however, each neuron in one group inhibits all neurons in the other group. In the study we use a dynamical map model with stochastic perturbations in which an isolated element (neuron) exhibits occasional spikes at random moments of time; however, the interaction between two groups of such elements leads to the formation of the mean activities of the groups in antiphase burstlike oscillations.

II. INDIVIDUAL SPIKING DYNAMICS

As a simple model for capturing the dynamics of the spiking activity of a neuron we use the following two-dimensional discrete-time system [21,22]:

$$\begin{aligned} x_{n+1} &= x_n + F(x_n) - y_n - \beta H(x_n - d) + I_n^{\mathrm{syn}}, \\ y_{n+1} &= y_n + \varepsilon(x_n - J), \end{aligned} \tag{1}$$

where x mimics the qualitative behavior of the neural membrane potential and y models the effects of relatively slow ionic currents governing the transient behavior of the neuron. The nonlinear functions $F(x)$ and $H(x)$ are written

$$F(x) = x(x - a)(1 - x), \tag{2}$$

$$H(x) = \begin{cases} 1, & x \geqslant 0 \\ 0, & x < 0, \end{cases} \tag{3}$$

*olmaov@neuron.appl.sci-nnov.ru

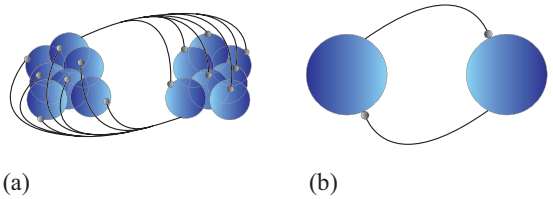

(a) (b)

FIG. 1. (Color online) Examples of symmetric reciprocally inhibiting networks, the half-center oscillators. (a) Two groups of neurons inhibiting each other. For simplicity, synaptic links from only one presynaptic neuron in each group are shown. (b) Similar network with only two neurons.

where $0 < a < 1$. The parameters β and d control the shape of bursting oscillations, ε is a time scale for y, and J defines neural excitability. For $J < J_{\min}$, where $J_{\min} = (1 + a - \sqrt{1 - a + a^2})/3$ and the function $F(x)$ has a minimum at $x = J_{\min}$ [Fig. 2(a)], the neuron is in a resting state (excitable regime). In contrast, for $J > J_{\min}$ the neuron generates spike sequences and the larger J is, the more spikes in a sequence.

Coupling between the neurons is modeled using the input synaptic current I_n^{syn} as defined by

$$I_n^{\text{syn}} = -g_n\left(x_n^{\text{post}} - v\right), \tag{4}$$

where g is the synaptic conductance, x^{post} is the membrane potential of the postsynaptic neuron, and v is the reversal potential. The dynamics of the synaptic conductance g is triggered by a presynaptic spike and relaxes in accordance with the dynamics of the following one-dimensional iteration process (a map):

$$g_{n+1} = \gamma g_n + (1 - \gamma) g_{\max} H(x_n^{\text{pre}} - \theta). \tag{5}$$

Here γ $(0 < \gamma < 1)$ defines a relaxation rate for the conductance, $g_{\max}$ is a maximum synaptic conductance, and θ is a threshold parameter. Such a model reflects the main dynamic properties of a real chemical synapse [25]. When a presynaptic neuron displays only subthreshold behavior, a synapse is silent, thus a postsynaptic neuron does not receive any input current from that neuron. In the opposite case, when the presynaptic neuron shows some activity above the threshold, e.g. fires action potentials, the synapse affects the postsynaptic neuron. Transitions between subthreshold activity and spiking of the presynaptic neuron result in switching off and on of the synapse with some rate of transient captured by (5). In terms of variables, when the value of the presynaptic membrane potential x_n^{pre} is above θ, the map (5) has a unique stable fixed point $g^* = g_{\max}$ and the value of g_n tends towards g^* exponentially with the rate $1 - \gamma$. This produces synaptic current for postsynaptic neuron [see (4)]. When $x_n^{\text{pre}} < \theta$, a trivial stable solution in (5) $g^* = 0$; after g approaches this state the neurons are uncoupled. Thus the variable g varies within the interval $0 < g < g_{\max}$ attracting alternately to $g^* = 0$ and $g^* = g_{\max}$, demonstrating transient dynamics with the rate $1 - \gamma$.

In order to model stochastic spiking of individual neurons we set the parameter values $a = 0.1$, $\varepsilon = 10^{-4}$, $\beta = 0.5$, and $d = 0.4$ and choose the values of the parameter J within the interval (0.03,0.049). Under these conditions the model reproduces the excitable regime, i.e., it does not generate

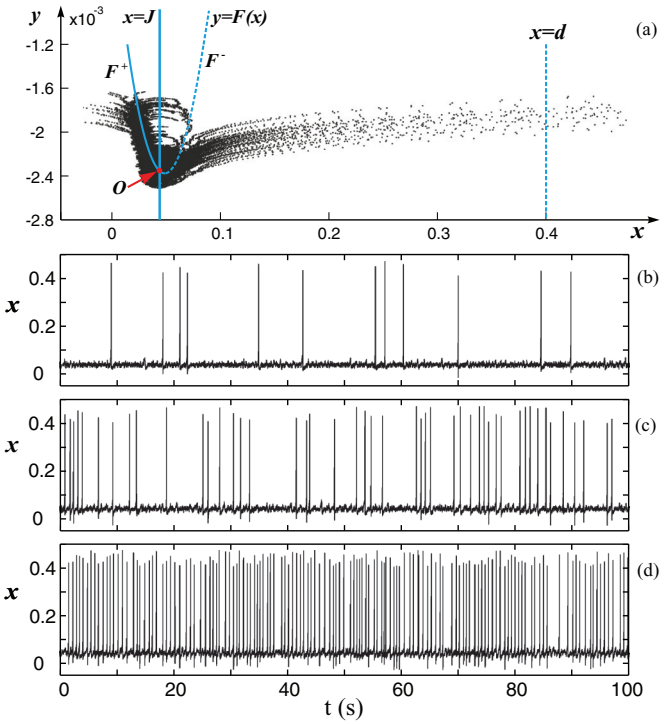

FIG. 2. (Color online) (a) Phase portrait of the map (1) for $a = 0.1$, $\varepsilon = 10^{-4}$, $\beta = 0.5$, $d = 0.4$, and $J = 0.04$. (b)–(d) Waveforms of the map (1) for (b) $J = 0.04$, (c) $J = 0.044$, and (d) $J = 0.048$.

any action potentials if it does not receive any external perturbations (an input current). If the external perturbation pushes the model state above the threshold value, the model generates an action potential and then returns to an equilibrium state. To generate spikes at random moments of time we add a term I_n^{rand} to the first equation of (1). The input sequence I_n^{rand} is a white Gaussian noise with zero mean and a standard deviation σ_{cur} equal to 0.001.

A phase portrait illustrating the trajectories of stochastic spiking is shown in Fig. 2(a). One can see that the system has a unique stable fixed point O [the crossing of the nullclines: the curve $y = F(x)$, consisting of two branches (left F^+ and right F^-), and the line $x = J$]. A trajectory moves in the neighborhood of O while the noise intensity is small enough. When the noise generates some high values, the trajectory reaches the discontinuity line $x = d$ and returns to F^+. Such a phase trajectory corresponds to a spike generation.

When model (1) with such properties receives a fluctuating input current I_n^{rand}, the model generates a sequence of spikes at random moments. Depending on the value of J and on the noise intensity σ_{cur}, there can be irregular sequences with different mean spike frequencies. Figures 2(b)–2(d) show waveforms for the same noise level and for three different values of the threshold parameter J. In this example we choose the sampling frequency equal to 1000 (i.e., we regard 1 s to be equal to 1000 iterations). It is seen that the larger J is, the higher the average spike frequency. This dynamics of spiking rate is summarized in Fig. 3, where the average spike rate $\langle R \rangle$ as a function of J is plotted for several noise intensities σ_{cur}. One can see that the sharp transition from silence to spike generation observed in the pure deterministic case ($\sigma_{\text{cur}} = 0$)

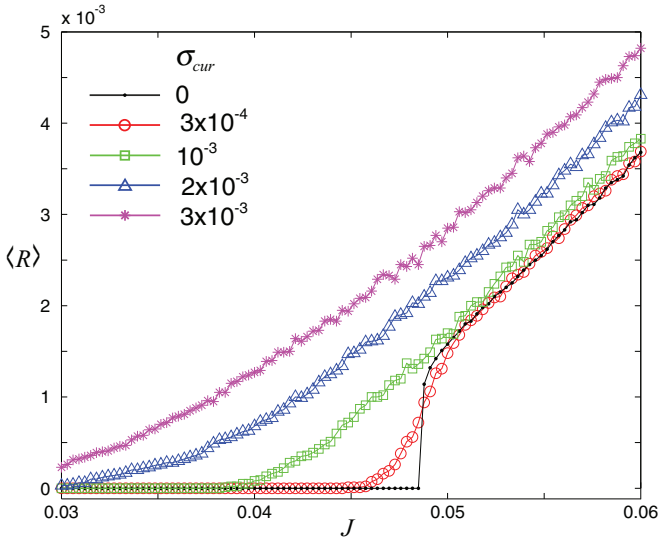

FIG. 3. (Color online) Spike rate $\langle R\rangle$ versus the threshold parameter J for different levels of the additive noise $\sigma_{\rm cur}$.

smoothes out into a monotonic increase of $\langle R\rangle(J)$ when noisy input is applied and increased.

A crucial dynamical property of neuron model required in our study is the ability of model to replicate the effect of PIR, which is a generation of a spike or a burst of spikes after the action of a hyperpolarizing stimulus, for example, $I_n^{\rm syn} = -A$, with $t_0 \leqslant n \leqslant t_1$ and $A > 0$. This property is achieved through the appearance of a new (shifted) nullcline $y = F(x) - A$ located below $y = F(x)$ in the phase plane during stimulation $t_0 \leqslant n \leqslant t_1$. As a result, a new stable fixed point $\widetilde{O}$ appears below O during this time. A disturbed trajectory moves to the left from the point $[J_{\rm min}, F(J_{\rm min})]$, providing hyperpolarization, and then follows down the curve $y = F(x) - A$ until the stimulus terminates. After that the nullcline $y = F(x)$ and point O return to the phase plane. The trajectory does not return to the equilibrium O directly, but quickly moves towards the line $x = d$ and after one or several jumps around $x = d$ returns to F^+. The resulting trajectory forms a spiking response to the inhibitory stimulus. Figure 4 shows neural responses produced by the model in reaction to negative pulses of input currents with different duration. The strength of PIR activity is proportional to the number of spikes in the evoked burst. As one can see, the longer the model gets

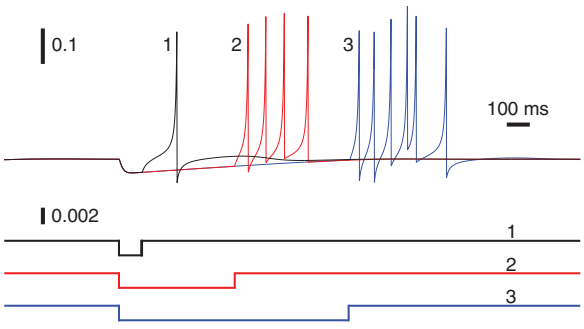

FIG. 4. (Color online) Effect of bursting rebound. After an inhibitory constant external current terminating, the neuron generates a spike or sequence of them depending on the duration and value.

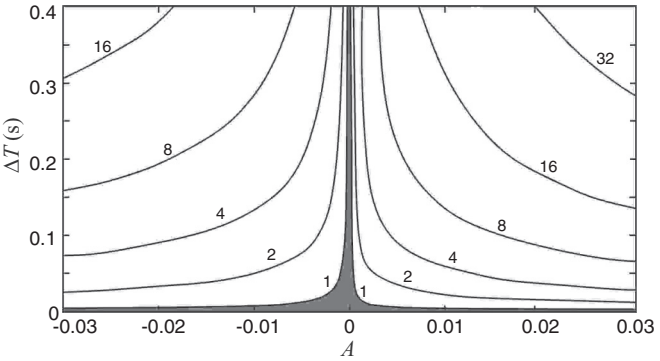

FIG. 5. Number of spikes in the neural response to a rectangular stimulus with amplitude A and duration $\triangle T$. The threshold parameter is $J = 0.044$.

hyperpolarized, the stronger the effect of PIR activity. The mechanism underlying such an effect is the following. For longer stimuli, the trajectory in the phase plane (x, y) spends more time moving down the shifted nullcline $y = F(x) - A$ and reaches a lower point before the stimulus terminates. This results in a lower starting point for moving up when the trajectory jumps around the discontinuity line $x = d$. The lower the trajectory begins moving up, the more jumps around $x = d$ it makes and the more spikes in a corresponding burst. Note that for a long enough hyperpolarizing stimulus the trajectory reaches the disturbed fixed point so further prolongation no longer affects the number of spikes in a response.

The analysis of transient spiking activity caused by PIR for a hyperpolarizing stimulus and spike generation for a depolarizing stimulus is summarized in Fig. 5. The numbers next to the border indicate the number of spikes produced by the stimuli. Only some borders corresponding to 2^N spikes are shown. The general conclusion of this analysis is that the longer the duration $\triangle T$ of a rectangular stimulus and/or the larger the absolute magnitude A, the more spikes are generated in a sequence for both hyperpolarizing ($A > 0$) and depolarizing ($A < 0$) stimuli (see Fig. 5). A narrow region (colored gray) covers the parameter values for which there is no spike generated in the model response.

III. GROUP DYNAMICS

To discuss the population dynamics let us consider a network of two groups, each of which contains 100 neurons as described above. A qualitative scheme of coupling between the groups is illustrated schematically in Fig. 1(a), where each neuron in one group inhibits all neurons in the other group and vice versa.

The diversity of neurons in each group is introduced by dispersion of the baseline states controlling the excitability properties, i.e., by the values of J that are taken to be normally distributed with mean $J_{\rm mean}$ ($0 < J_{\rm mean} < 0.1$) and standard deviation $\sigma_J = 10^{-2}$. In this case the elements individually generate stochastic spikes with different mean firing rates. Coupling into the network [Fig. 1(a)] evokes a new type of collective behavior in the form of antiphase oscillations that produce regular modulation of group activities. As will be

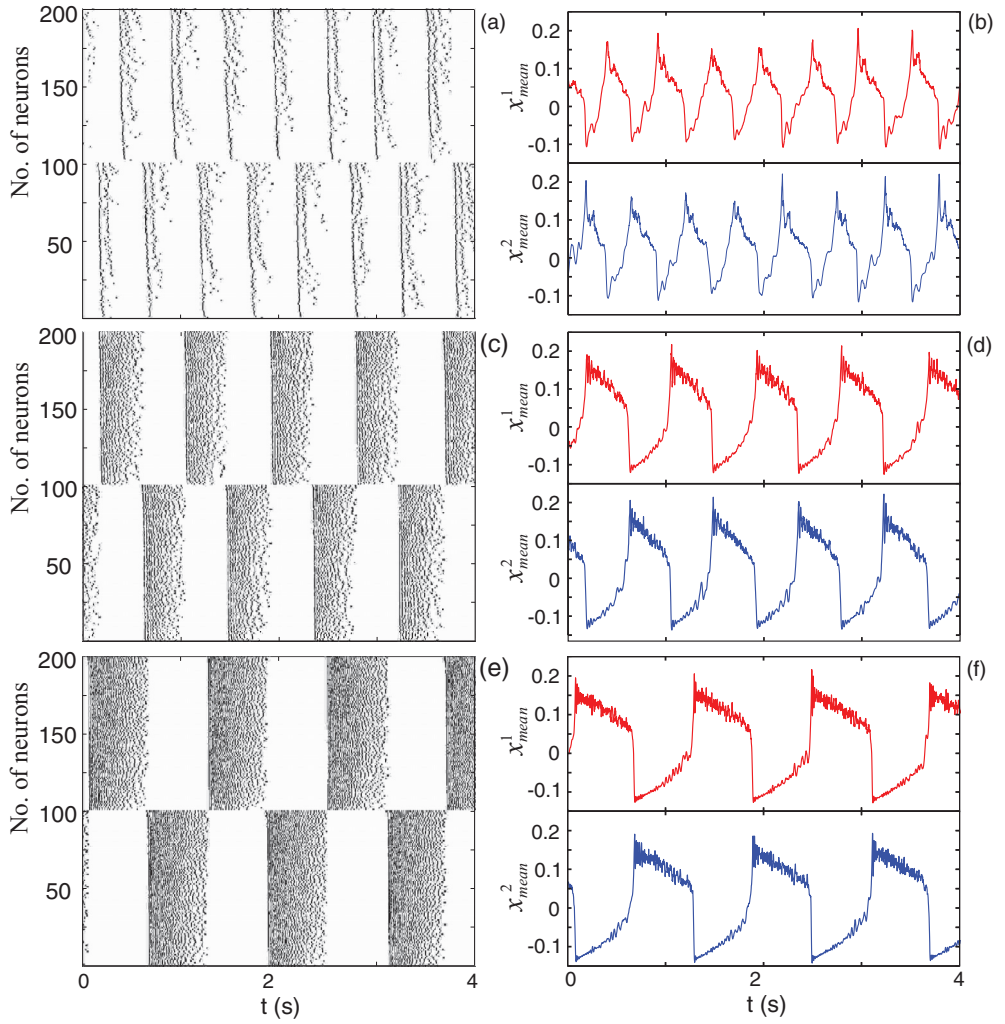

FIG. 6. (Color online) (a), (c), and (e) Rastrograms of the spiking activity in two neuron groups consisting of 100 elements each and (b), (d), and (f) corresponding waveforms of the average activity. The three cases presented differ by the mean excitability level: (a) and (b) $J_{\text{mean}} = 0.03$, (c) and (d) $J_{\text{mean}} = 0.05$, and (e) and (f) $J_{\text{mean}} = 0.07$. The standard deviation is $\sigma_J = 10^{-2}$ and the maximum coupling $g_{\text{max}} = 5 \times 10^{-3}$ in all cases.

shown below, these oscillations of the system respond to an external stimulation in a predictable manner.

A. Emergent bursting

First we consider the collective dynamics of the network operating autonomously. The results of network simulations in this case are shown in Fig. 6 for different levels of mean excitability J_{mean} of the network population. Figures 6(a), 6(c), and 6(e) show the occurrence of spikes in both groups. One can see that irregular action potentials of one group arise in time intervals that do not overlap with those of another group, causing the alternation of group activities. Therefore, the waveforms of the average activities of the two groups are antiphase bursts [Figs. 6(b), 6(d), and 6(f)]. It is also shown that an increase of the value of J_{mean} leads to an increase of the bursting period.

To study how the excitability level of the network and the strength of inhibitory coupling affect the parameters of collective activity, we have calculated spectrograms of group bursting oscillations for different J_{mean} and g_{max}. We set the sampling frequency equal to 500. The main results are illustrated in Figs. 7(a) and 7(b), which present two different values of the coupling strength g_{max}. One can clearly see that there is a threshold value of J_{mean} corresponding to the emergence of bursting activity. This threshold level decreases as the value of g_{max} increases. Another property of these oscillations is that the average bursting frequency decreases with an increase of the excitation level of the network, J_{mean}.

The results are summarized in Figs. 7(c) and 7(d), where the bursting rate and the level of activity within each burst are shown in the parameter plane $(J_{\text{mean}}, g_{\text{max}})$. We measure the burst rate as an average number of group bursts per second. Note that the number of individual spikes per group burst increases with increasing J_{mean} and/or g_{max}, as seen in Fig. 7(d). The white areas in Figs. 7(c) and 7(d) correspond to the no-bursting regimes that take place below the network threshold level discussed above.

To complete the description of the group dynamics in the half-center oscillator network we examine the average

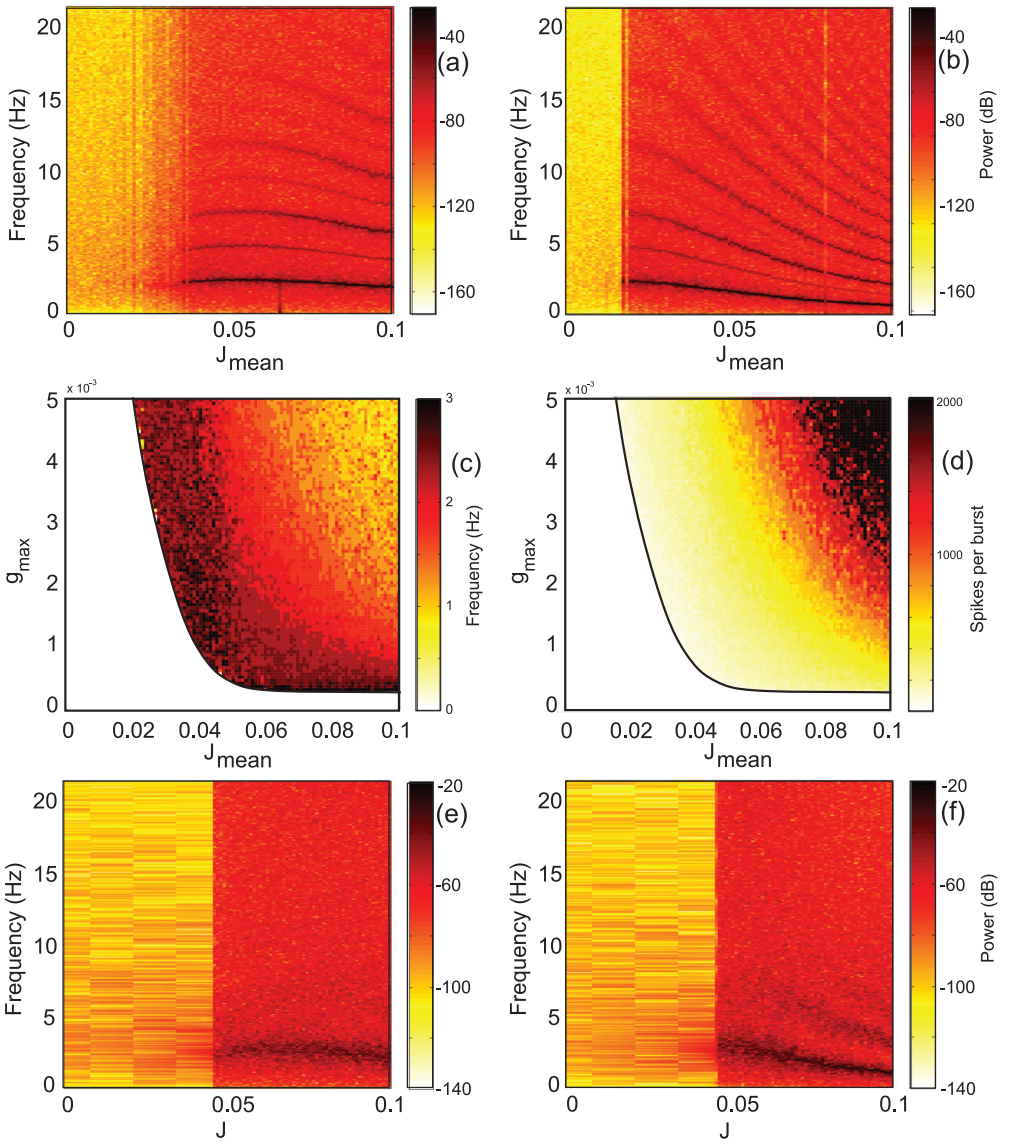

FIG. 7. (Color online) Spectrograms of group bursting for (a) $g_{\max} = 10^{-3}$ and (b) $g_{\max} = 5 \times 10^{-3}$, with $\sigma_J = 10^{-2}$. (c) Average bursting frequency and (d) average number of individual spikes per group burst, depending on the mean excitability level J_{mean} and the average maximum conductivity $g_{\max}$. Also shown are spectrograms of one of the two coupled spiking neurons with the same parameters for (e) $g_{\max} = 0.1$ and (f) $g_{\max} = 0.5$.

group behavior using its trajectories in the phase space analysis. Consider how a representative point (x_n^{mean}, y_n^{mean}) where $(x_n^{mean} = \sum_{k=1}^{N} x_n^{(1)}, y_n^{mean} = \sum_{k=1}^{N} y_n^{(1)})$ moves in the projection on the plane (x, y). Here $N = 100$ is the number of neurons in one group. To be specific, we take the first group [which is indicated by the index (1)]; for the second group the result will be the same due to the symmetry of the network configuration. Figure 8 shows that such averaged trajectories form a noisy limit cycle attractor that evolves with increasing values of J_{mean}, getting closer to the limit cycle typical for the cases of fast and slow oscillations in a low-dimensional system.

An interesting question that we address in this study is how the model of such a large network of reciprocally inhibiting groups of neurons can be replaced with a pair of reciprocally inhibiting neurons. Further, we ask whether the neurons in the pair have parameters similar to the neurons in the group. Here we will demonstrate a simple case in which the network consists of just two spiking neurons mutually inhibiting each other. The parameters of the neurons are set to be the same as the mean parameters of the neurons used in a group. The simulations show that there are no such pronounced oscillatory properties in Fig. 8(d) and the bursting in the corresponding spectrograms look rather faded with different dynamics of the threshold [see Figs. 7(e) and 7(f)]. The neurons that produce a robust rhythm of bursting operating in networks generate irregular bursts with fluctuating duration operating in the case of a reduced network model. We will focus more on this comparative analysis in the remainder of the paper.

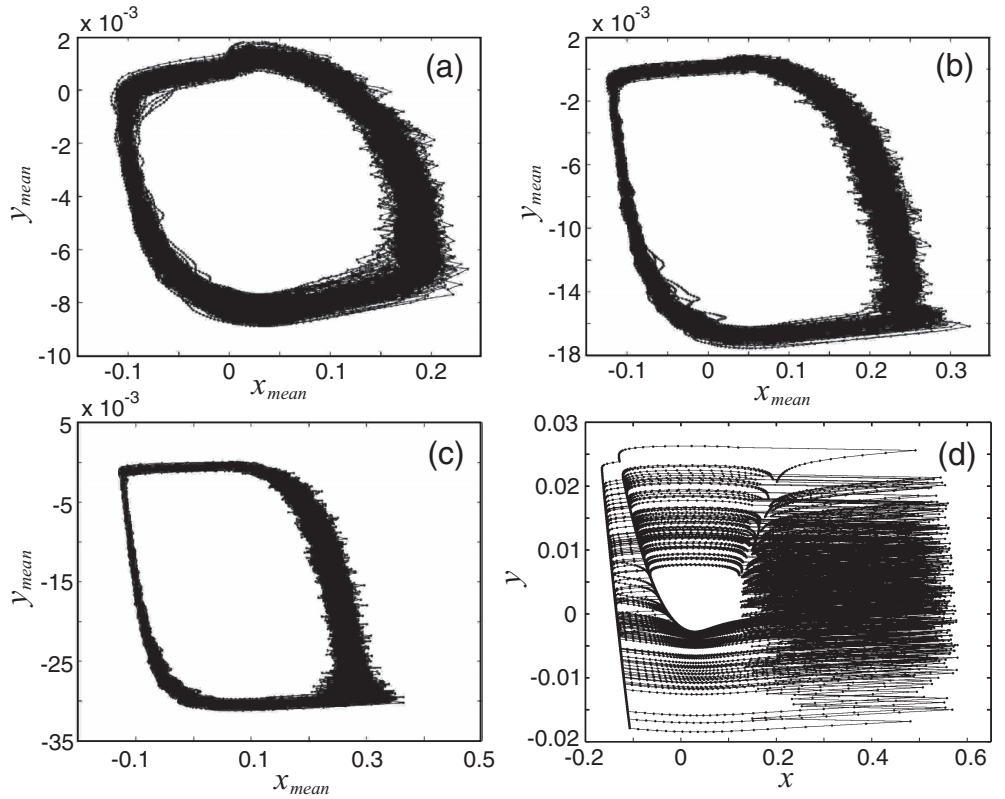

FIG. 8. Averaged trajectory $(x_n^{\text{mean}}, y_n^{\text{mean}})$ over $N = 100$ neurons in one group for $g_{\max} = 5 \times 10^{-3}$ and different values of J_{mean}: (a) 0.03, (b) 0.05, and (c) 0.07. (d) Phase portrait corresponding to one neuron in a pair of reciprocally inhibiting spiking neurons; the parameters are $g_{\max} = 0.3$ and $J = 0.05$.

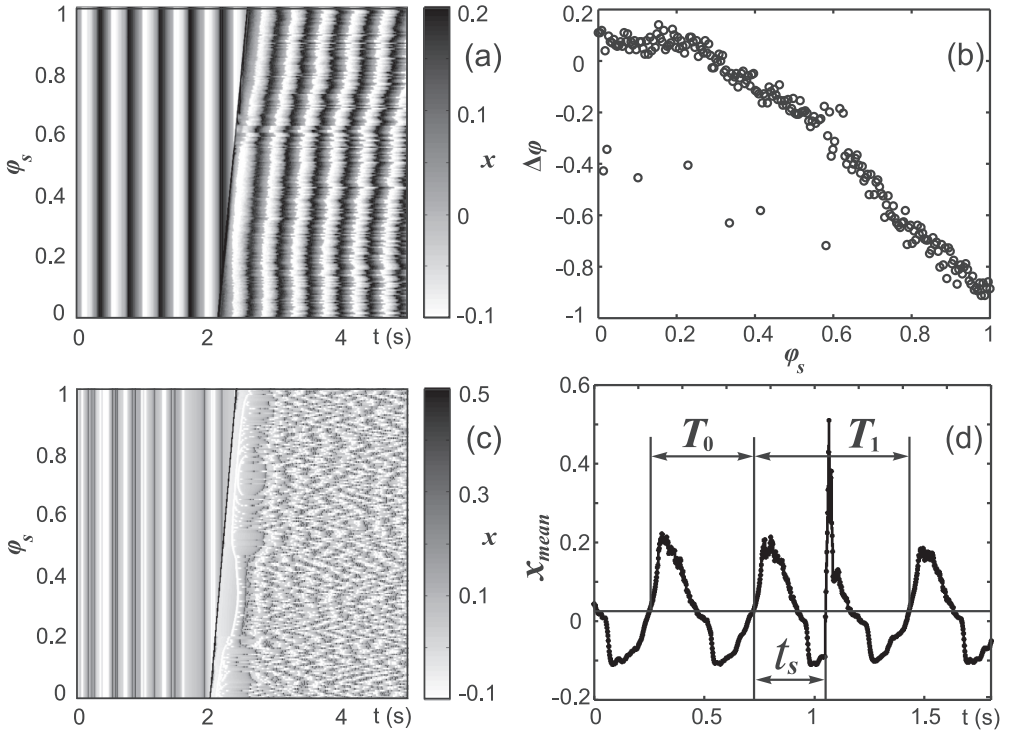

FIG. 9. (a) Phase reset in two reciprocally inhibiting groups. The average activity of one group is shown for different moments of stimulation. (b) Corresponding phase resetting curve. (c) Stimulation of one neuron in a pair of reciprocally inhibiting spiking neurons. Note that a new phase depends on a moment of stimulation in a rather chaotic manner. (d) Definition of phase resetting.

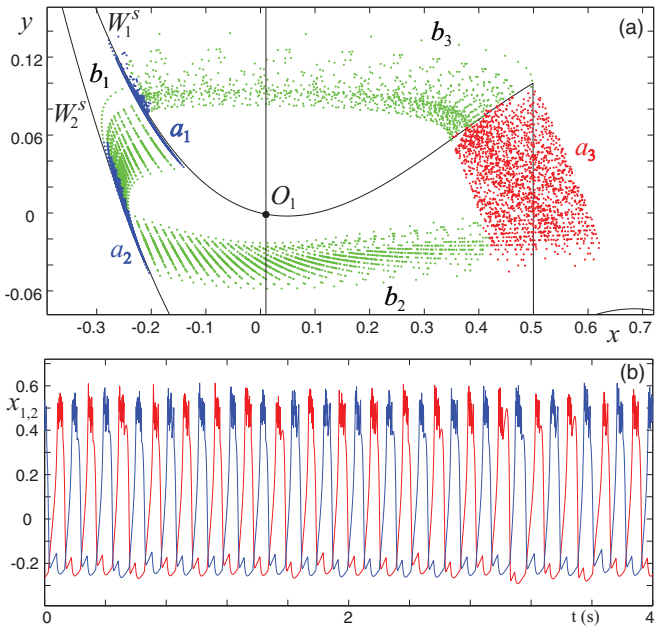

FIG. 10. (Color online) (a) Phase portrait of one neuron in the mutually inhibiting couple (6) and (b) corresponding waveforms of spike-bursting neurons.

B. Phase reset

One of the most important elements in capturing the behavior of CPGs is the dynamics of its response to the external sensory or control stimulus. In the case of the half-center oscillator network this dynamics is related to the phase reset properties. Considering the effects of phase reset in the network, we apply a short stimulus with $A = -0.01$ and $\triangle T = 20$ ms to all the elements in one group and examine the phase of new bursting oscillations after the transient is complete. Figure 9(a) shows that the network responds differently depending on the network state when it receives a stimulus. There are some moments (during the active phase of bursts) when the stimulus hardly disturbs the network oscillations; however, there are moments (during the passive phase of bursts) when the stimulus can lead to a significant phase shift. To quantify this property we plotted the phase resetting curve (PRC) (see, e.g., [26]) shown in Fig. 9(b). We define the phase of stimulation as $\varphi_s = t_s/T_0$ and the phase difference after the reset as $\triangle\varphi = (T_0 - T_1)/T_0$ [see Fig. 9(d)]. Note that in the case of a reduced network model with only a pair of spiking reciprocally inhibiting neurons with the same intrinsic behavior as the neurons in a group, the post-transient oscillations have no clear reset phase and the reset curve observed for the large network is not reproduced [Fig. 9(c)].

IV. REDUCTION TO A PAIR OF BURSTING NEURONS

We have shown above that the emergence of antiphase bursts in the interacting groups cannot be reduced to the dynamics of two interacting spiking elements (see Figs. 7 and 8). Nor can the phase reset effect be explained by considering only a pair of neurons (Fig. 9) that generate irregular spikes.

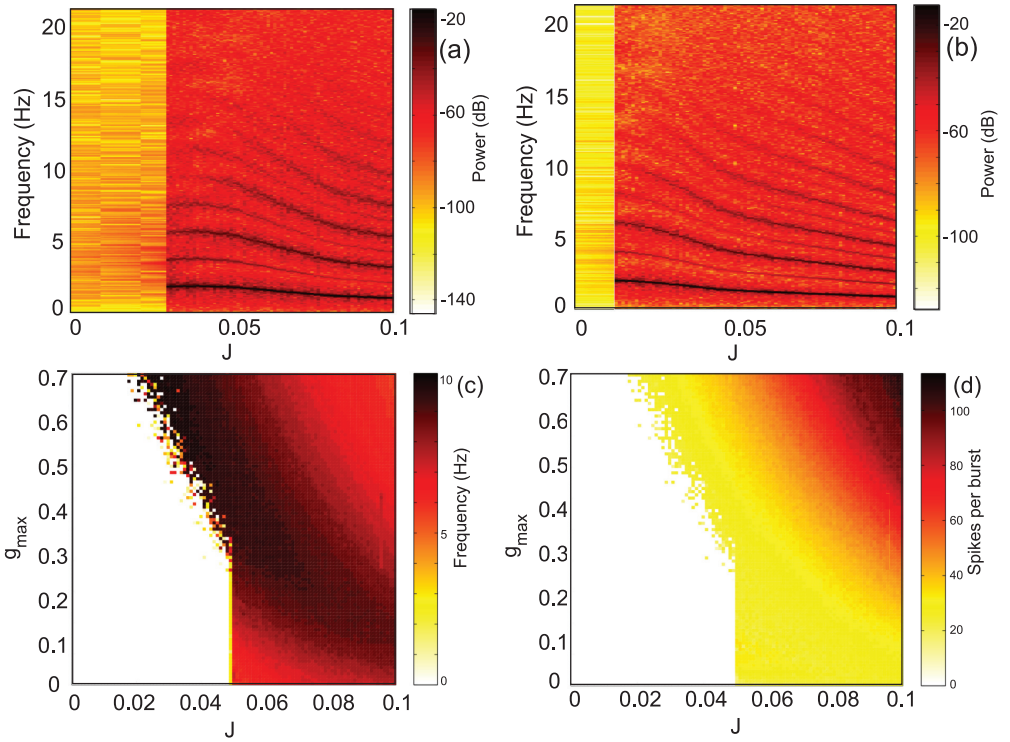

FIG. 11. (Color online) Spectrograms for one of the two coupled bursting neurons for (a) $g_{max} = 0.3$ and (b) $g_{max} = 0.7$, with $\beta = 0.2$, $d = 0.5$, and $\varepsilon = 0.002$. (c) Bursting frequency and (d) average number of spikes per burst as functions of J and g_{max}.

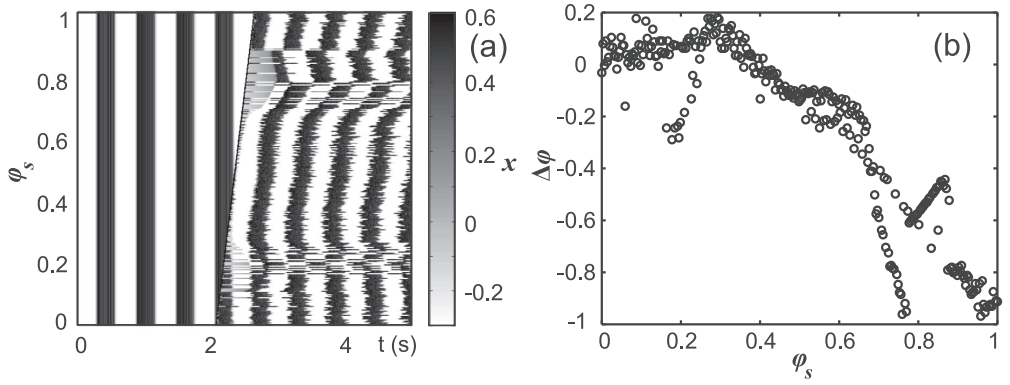

FIG. 12. (a) Phase reset in two reciprocally inhibiting bursting neurons. The activity of one neuron is shown for different moments of stimulation. (b) Corresponding phase resetting curve.

However, if one wishes to study a complex network including more than two large populations, it is useful to find reduced models where the group dynamics can be approximated by the dynamics of some simple unit. In our case, it is reasonable to consider two mutually inhibiting neurons [Fig. 1(b)] with spike-bursting behavior that is observed in the group average activity [Figs. 6(b), 6(d), 6(f), and 8(a)–8(c)]. To replicate this regime, we choose values of β and d in such a way that each neuron generates a sequence of spikes (a burst).

Thus we have the following map describing the dynamics of the two coupled neurons:

$$\begin{aligned} x_{n+1}^{(i)} &= x_n^{(i)} + F\left(x_n^{(i)}\right) - y_n^{(i)} - \beta H\left(x_n^{(i)} - d\right) + I_n^i, \\ y_{n+1}^{(i)} &= y_n^{(i)} + \varepsilon\left(x_n^{(i)} - J\right), \quad I_n^{(i)} = -g_n^{(i)}(x_n^{(i)} - \nu), \\ g_{n+1}^{(i)} &= \gamma g_n^{(i)} + (1-\gamma) g_{\max} H(x_n^{\mathrm{pre}} - \theta), \end{aligned} \tag{6}$$

where the index i ($i = 1,2$) denotes the first and the second neuron and pre corresponds to a presynaptic neuron (the first neuron is presynaptic for the second one and vice versa). We set $a = 0.1, \varepsilon = 0.002, \beta = 0.2, d = 0.5, \gamma = 0.5, \nu = -0.6$, and $\theta = 0.15$ and take J from the interval (0,0.1) and $g_{\max}$ from the interval (0,0.7).

The phase portrait for one neuron in the pair is shown in Fig. 10(a) and corresponding waveforms for both elements are shown in Fig. 10(b). Note that the effect of one element on the other can be described in terms of switching between two phase portraits in the phase plane (x,y) corresponding to a single element dynamics. When the postsynaptic neuron (to be specific, consider the first one) is isolated, i.e., the presynaptic neuron is below the threshold value $x_n^{\mathrm{pre}} < \theta$ and does not inhibit the first one, the dynamics in (x,y) is determined by the stable fixed point O_1 and the stable invariant curve W_1^s. During this stage phase trajectories are in the area a_1. When the postsynaptic neuron is under inhibition, i.e., the presynaptic neuron is over the threshold $x_n^{\mathrm{pre}} > \theta$, the dynamics in (x,y) is governed by another stable invariant curve W_2^s [Fig. 10(a)] and phase trajectories enter the area a_2. After this stage terminates, the trajectories leave a_2 and move to a_3 and this motion determines the PIR burst. After many repetitions of these switchings we have the waveforms of two antiphase bursting oscillations shown in Fig. 10(b).

As we did for the network dynamics in Sec. III, now we analyze the influence of the excitability level and the coupling intensity on the bursting properties. We calculate spectrograms for different J and $g_{\max}$. The results are shown in Figs. 11(a) and 11(b) for two different values of the coupling strength. It is seen that there is a threshold value of J corresponding to the bursting appearance and it becomes lower for increasing $g_{\max}$ [see Figs. 7(a) and 7(b)].

The bursting rate and the number of spikes per burst as functions of J and $g_{\max}$ are shown in Figs. 7(c) and 7(d), respectively. A remarkable feature is the qualitative similarity of these characteristics with those of group bursts [see Figs. 7(c) and 7(d)]. There are threshold values of burst generation and the larger J and $g_{\max}$ result in smaller burst frequencies and the greater number of spikes per burst. The main difference with Figs. 7(c) and 7(d) is that for $J > J_{\min} \approx 0.05$ there is no lower $g_{\max}$ threshold for burst generation because in this regime neurons generate bursts in the individual dynamics.

The phase reset effect for two bursting neurons (Fig. 12) is similar to that of the groups [Figs. 9(a) and 9(b)], except that now the PRC has a ruptured shape due to the bursting nature of the individual element, which has larger variation of sensitivity to the stimulus at different phases of burst.

V. CONCLUSION

We have considered the collective behavior of two reciprocally coupled populations of spiking neurons. This system provides a basis for the functioning of many CPGs. We found that stochastic spiking elements with the PIR property, when coupled into such a network, exhibit emergent antiphase bursts in the average group activity. It should be noted that the emergence of bursting behavior in large neural networks of nonbursting elements takes place not only in systems with reciprocal inhibition. There may be other dynamic or structural mechanisms of this activity. For example, in [27] the collective bursting behavior was found in a large network of intrinsically nonbursting neurons. The mechanism responsible for the bursting is a combination of excitatory feedback received from neighboring neurons together with an activity-dependent adaptation mechanism that slows down spiking. Another example is a population of nonbursting cells coupled via the mean field [28]. It was shown in such a system that emergent bursting is due to coupling alone and is very robust to changes

in the coupling strength and that heterogeneity in the model parameters does not play a role.

We have shown that the nonlinear collective dynamics of a large-scale network can be studied in some aspects by means of a simplified model. The dynamic similarity between group averaged activity and spike-bursting single-element behavior allows us to analyze the emergence of antiphase bursting and the properties of phase reset in a pair of mutually inhibiting bursting units. Another supporting detail is that in the network model irregular spikes appear due to the PIR and in the reduced model bursts alternate due to the same mechanism.

A reduction of the network activity to simplified (mean-field) models describing average dynamics has been utilized for biological networks [29–31]. A common requirement for applying this method is that a network does not have complex connectivity structure. In our network consisting of two homogeneous subnetworks, the *ad hoc* reducing procedure is based on similar phase portraits that lead to similar phase resets. The result obtained provides a starting point for modeling multipopulation networks of CPGs. Interaction and synchronization mechanisms for network functioning can be basically understood in terms of average-activity units.

ACKNOWLEDGMENTS

This research was sponsored by the Ministry of Education and Science of the Russian Federation (Projects No. 8497 and No. 14.132.21.1354) and the Russian Foundation for Basic Research (Projects No. 12-02-00526, No. 13-02-00858, No. 12-04-31963, and No. 12-02-31252). N.F.R. was partially supported by ONR Grant No. N00014-07-1-0741.

[1] T. H. Bullock, Behaviour **17**, 48 (1961).
[2] D. M. Wilson and R. J. Wyman, Biophys. J. **5**, 121 (1965).
[3] F. Delcomyn, Science **210**, 492 (1980).
[4] R. M. Harris-Warrick and B. R. Johnson, in *Perspectives in Neural Systems and Behavior*, edited by T. Carew and D. Kelley (Alan R. Liss, New York, 1989), pp. 51–72.
[5] Yu. I. Arshavsky, I. N. Beloozerova, G. N. Orlovsky, Yu. V. Panchin, and G. A. Pavlova, Exp. Brain Res. **58**, 273 (1985).
[6] S. Grillner, Nat. Rev. Neurosci. **4**, 573 (2003).
[7] J. T. Buchanan, Biol. Cybern. **66**, 367 (1992).
[8] J. T. Buchanan, Prog. Neurobiol. **63**, 441 (2001).
[9] A. Doloc-Mihu and R. L. Calabrese, J. Biol. Phys. **37**, 263 (2011).
[10] D. A. McCrea and I. A. Rybak, Brain. Res. Rev. **57**, 134 (2008).
[11] G. S. Cymbalyuk, Q. Gaudry, M. A. Masino, and R. L. Calabrese, J. Neurosci. **22**, 10580 (2002).
[12] P. A. Guertin, Brain Res. Rev. **62**, 45 (2009).
[13] E. Marder and D. Bucher, Curr. Biol. **11**, R986 (2001).
[14] S. Coombes and S. H. Doole, Phys. Rev. E **54**, 4054 (1996).
[15] A. J. Ijspeert, Neural Netw. **21**, 642 (2008).
[16] J. Ayers, N. Rulkov, D. Knudsen, Y.-B. Kim, A. Volkovskii, and A. Selverston, Appl. Bion. Biomech. **7**, 57 (2010).
[17] J. Ayers and N. Rulkov, in *Bio-mechanisms of Animals in Swimming and Flying*, edited by N. Kato and S. Kamimura (Springer, Tokyo, 2007), pp. 295–306.
[18] A. Westphal, N. F. Rulkov, J. Ayers, D. Brady, and M. Hunt, Smart Struct. Syst. **8**, 39 (2011).
[19] M. Courbage and V. I. Nekorkin, Int. J. Bifurcat. Chaos **20**, 1631 (2010).
[20] B. Ibarz, J. M. Casado, and M. A. F. Sanjuán, Phys. Rep. **501**, 1 (2011).
[21] V. I. Nekorkin and L. V. Vdovin, Izv. Vyssh. Uchebn. Zaved. Prikladn. Nelinejn. Din. **15**, 36 (2007).
[22] M. Courbage, V. I. Nekorkin, and L. V. Vdovin, Chaos **17**, 043109 (2007).
[23] N. F. Rulkov, Phys. Rev. E **65**, 041922 (2002).
[24] N. F. Rulkov, I. Timofeev, and M. Bazhenov, J. Comput. Neurosci. **17**, 203 (2004).
[25] A. Destexhe, Z. M. Mainen, and T. J. Sejnowski, in *Methods in Neuronal Modeling*, 2nd ed., edited by C. Koch and I. Segev (MIT Press, Cambridge, 1998), pp. 1–26.
[26] E. M. Izhikevich, *Dynamical Systems in Neuroscience: The Geometry of Excitability and Bursting* (MIT Press, Cambridge, 2005), Chap. 10.
[27] D. A. Blank and R. Stoop, Z. Naturforsch. Teil A **54**, 617 (1999).
[28] G. de Vries, Phys. Rev. E **64**, 051914 (2001).
[29] J. Tabak, M. Mascagni, and R. Bertram, J. Neurophysiol. **103**, 2208 (2010).
[30] B. Vladimirski, J. Tabak, M. O'Donovan, and J. Rinzel, J. Comput. Neurosci. **25**, 39 (2008).
[31] Y. Wu, W. Lu, W. Lin, G. Leng, and J. Feng, PLoS ONE **7**, e38402 (2012).